Proceedings of the Seventh International Conference on
Railway Technology: Research, Development and Maintenance
Edited by: J. Pombo
Civil-Comp Conferences, Volume 15, Paper 6.2
Civil-Comp Press, Edinburgh, United Kingdom, 2026
ISSN: 2753-3239, doi: 10.4203/ccc.15.6.2

Impact of Wheel Wear on the Nonlinear Bifurcation Mechanism of Wheelset Hunting Under the Characteristic Switch-Rail Profile

T. Li, J. Xu and P. Wang

**Southwest Jiaotong University,
Chengdu, People's Republic of China**

Abstract

Turnout zones, characterized by intricate wheel-rail contact geometry and dynamic load transfer, represent critical weak sections influencing vehicle running stability. With the continuous accumulation of service mileage in high-speed railways, wheel profile wear has become increasingly prominent, significantly altering wheel-rail contact relationships, especially in turnout areas, which may exacerbate nonlinear dynamic behavior and induce hunting instability. Focusing on the characteristic switch rail profile, this study establishes a nonlinear single-wheelset dynamic model incorporating equivalent conicity and flange forces, based on long-term field measurements of LMA-type wheel wear profiles. The Hopf bifurcation characteristics are systematically analyzed under different service mileages. Results show that increased mileage leads to a significant rise in equivalent conicity and a substantial reduction in bifurcation speed, dropping from 86.92 m/s at 50,000 km to 40.10 m/s at 200,000 km. Concurrently, the bifurcation type transitions from supercritical to subcritical, shifting the instability mechanism from continuous oscillation to a discontinuous jump-type phenomenon with hysteresis. Two-parameter bifurcation analysis further reveals that suspension stiffness and creep coefficients jointly govern the boundary of bifurcation types, which migrates systematically with wear progression. This study aims to elucidate the mechanisms by which wheel profile evolution dictates the nonlinear bifurcation behavior in turnout zones. It establishes a robust theoretical foundation and a bifurcation-oriented framework for optimizing switch-rail profiles, matching suspension parameters, and implementing mileage-dependent stability management throughout the operational lifecycle.

Keywords: wheel profile evolution, switch rails, equivalent conicity, Hopf bifurcation, hunting stability, subcritical instability.

1 Introduction

Turnouts, as indispensable infrastructure for route switching, represent the most vulnerable components within the track structure. Characterized by intricate structural configurations and complex wheel-rail coupling relationships, turnout zones exhibit a higher susceptibility to diverse defects compared to open tracks [1]. Unlike standard line sections, the rail geometry in turnout zones utilizes a composite structure comprising switch rails, wing rails, point rails, and stock rails, each featuring varying head widths and heights to facilitate the transition of wheel loads [2]. Induced by inherent structural irregularities, high-speed vehicles traversing turnout zones inevitably experience lateral displacements, which subsequently trigger hunting motion.

The wheel-rail contact relationship constitutes a primary nonlinear characteristic of the vehicle system. Variations in contact geometric parameters beyond specific critical thresholds dictate shifts in hunting stability, manifesting as bifurcation phenomena. Driven by the robust nonlinearity of the vehicle system, the underlying bifurcation mechanisms of hunting motion exhibit high complexity, generally categorized into two fundamental types. Figures 1(a) and (b) illustrate supercritical Hopf bifurcation, whereas Figure 1(c) depicts the subcritical Hopf bifurcation scenario. In these diagrams, solid lines denote stable equilibrium solutions and stable limit cycle trajectories, while dashed lines represent unstable branches. The velocity corresponding to the Hopf bifurcation point H is defined as the linear critical speed V_H, representing the stability threshold under idealized conditions. Conversely, point N identifies the nonlinear critical speed V_N, below which the vehicle system maintains absolute stability. In practical operational environments, the effective critical speed of the vehicle typically falls between V_H and V_N, as shown in Figures 1-2(b) and (c).

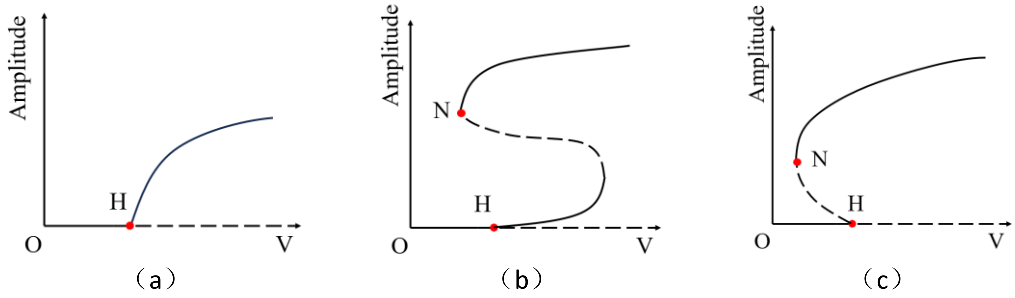

Fig. 1. Typical bifurcation modes in vehicle systems: (a) Supercritical Hopf bifurcation; (b) Supercritical Hopf bifurcation; (c) Subcritical Hopf bifurcation.

In recent years, significant scholarly attention has been devoted to the dynamic performance of vehicles negotiating turnouts under diverse wear conditions. Wang [3] developed a high-speed vehicle dynamics model coupled with the Jendel wear model to investigate the dynamic behavior and wear characteristics of high-speed trains. Hou[4] combined long-term field measurements of wheel/rail profiles with multibody vehicle-dynamics simulations in Simpack to examine how wheel-wear-driven contact-geometry evolution degrades high-speed train running stability and ride quality. Chen[5] coupled a vehicle-turnout dynamics model with CONTACT-based non-Hertz contact and shakedown analysis to assess how hollow-wear profile evolution influences wheel-rail interaction and rolling contact fatigue in high-speed turnouts. Hao [6] investigated the effects of flange wear on wheel-rail interaction by developing a coupled model of high-speed flexible turnouts and multi-rigid vehicles. Shi [7] conducted a two-year long-term on-track measurement campaign, using wheel-profile measurements and onboard vibration monitoring over 2 million km and multiple reprofiling cycles to quantify wheel-wear evolution and its effects on high-speed-train stability and ride comfort. Regarding nonlinear stability, Wang [8] explored the impact of wheel wear on the stability and frictional performance of freight wagon systems, unveiling the fundamental mechanisms of hunting motion and bifurcation. Furthermore, Liu [9] assessed the influence of individual measured wheel profiles on vehicle dynamics and conducted a comparative study of six computational methods for evaluating critical speeds.

Under the service environment of high-speed railways, wheel profile wear evolution has become increasingly prominent alongside the continuous rise in operating speeds, axle loads, and traffic density. Wear-driven microscopic profile alterations often induce drastic fluctuations in wheel-rail contact geometric nonlinearity, thereby deteriorating the running stability of the vehicle system and compromising operational safety. Consequently, it is of paramount importance to elucidate the mechanisms by which wheel profile evolution influences the lateral stability of nonlinear wheelset systems under actual service conditions and varying operational mileages.

While extensive research has focused on wheel wear and its induced nonlinear stability evolution on open tracks, studies addressing turnout sections remain comparatively scarce. To date, reports elucidating the underlying coupling between "time-varying wear evolution" and "turnout-specific nonlinear bifurcation mechanisms" are notably limited. Particularly under high-speed conditions, a systematic theoretical characterization and quantitative support regarding how geometric discontinuities in turnout zones intervene in Hopf bifurcation type transitions and the evolution of stability domain boundaries are still lacking. To address this, the present study utilizes field-measured multi-mileage wheel wear data to construct a single-wheelset dynamics model that incorporates nonlinear flange forces and accounts for the equivalent conicity of characteristic rail profiles in the switch zone. This framework systematically reveals the mechanisms through which wheel wear influences system bifurcation characteristics under specific switch rail profiles.

2 Methods

During vehicle transit, excessive lateral displacement of the wheelset induces contact between the wheel flange and the rail head, generating a lateral restoring force defined as the flange force. Given that the characteristic sections of the switch rail are primarily derived from the stock rail, they share a common gauge face with the stock rail. Consequently, this study employs the same flange force model used for open tracks. Specifically, an exponential model proposed in Reference [10] is implemented; this model provides a high-fidelity representation of actual flange force characteristics while preserving the integrity of the system's bifurcation type. The flange force model is illustrated in Figure 2, and the mathematical expression for the exponential model is as follows:

$$F_t = p_1 e^{q_1 y_w} - p_1 e^{-q_1 y_w} \tag{1}$$

Where $p_1 = -3.906\times10^{-4}$， $q_1 = -1645$。

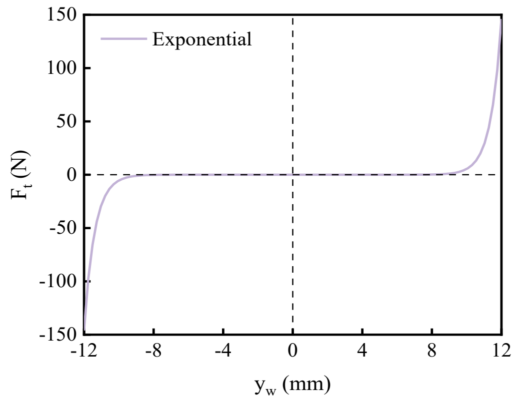

Fig. 2 flange force models

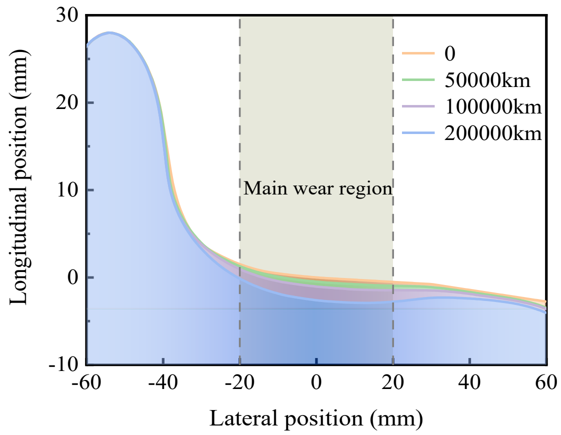

Fig. 3 LMA wheel profiles at various service mileages.

Longitudinal field monitoring was conducted to observe the evolution of hollow wear on LMA-type wheels of high-speed vehicles operating at a maximum speed of 350 km/h. Wheel profile data across various service mileages within the initial re-turning cycle were recorded, as illustrated in Fig. 3. The MiniProf measurement system and AutoCAD software were employed to precisely acquire and digitize the wheel profiles. Measurements were performed at three discrete circumferential locations on each wheel; the resulting data exhibited high consistency with only marginal measurement errors. Consequently, the mean of these three measurements was adopted as the representative profile for subsequent analysis. The empirical results indicate that wear development is primarily concentrated within the lateral range of -20 mm to 20 mm on the wheel tread, whereas wear in other regions of the profile is negligible.

Focusing on the 35 mm head-width characteristic profile, a section known for its relatively inferior lateral stability within the switch zone [2], this study quantified the equivalent conicity across varying service mileages. This analysis was performed using the field-measured worn wheel profiles and an equivalent conicity calculation method specifically established for turnout areas based on the wheelset hunting wavelength formula [11]. The wheel-rail contact relationships and the resulting equivalent conicity for each mileage stage are depicted in Fig. 4 and Fig. 5, respectively. Evidently, at a service mileage of 0 km, the equivalent conicity of the wheelset system is sustained at a low level of approximately 0.03 within the lateral displacement range of -8 mm to 8 mm. As service mileage accumulates, the equivalent conicity progressively augments alongside the evolution of wheel wear. This wear-induced increase in equivalent conicity becomes significantly more pronounced once the vehicle reaches or exceeds a service mileage of 100,000 km.

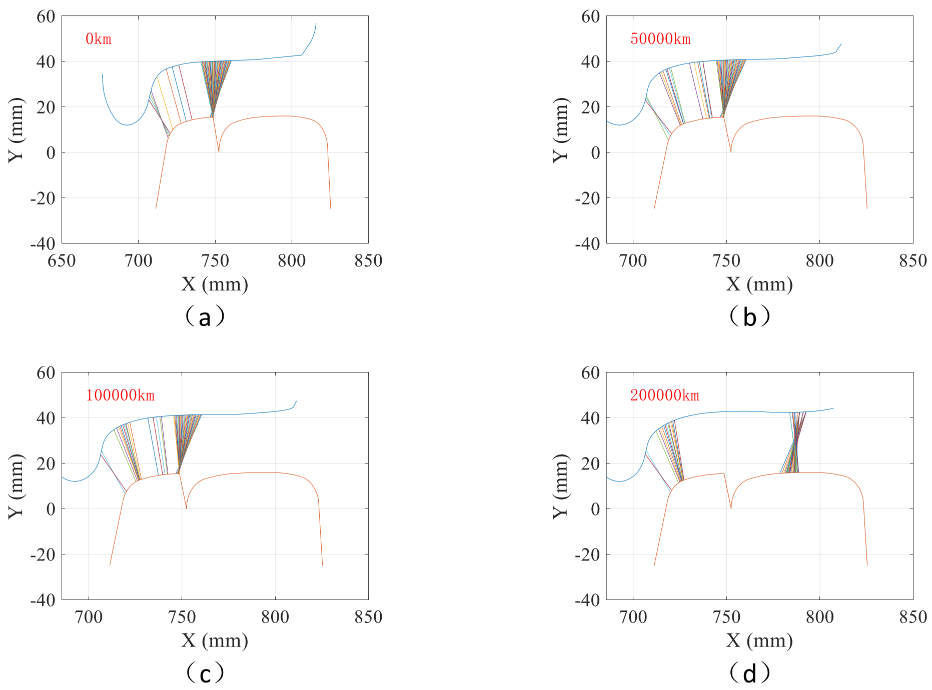

Fig. 4. Wheel-rail contact relationships at different service mileages: (a) 0 km; (b) 50,000 km; (c) 100,000 km; (d) 200,000 km.

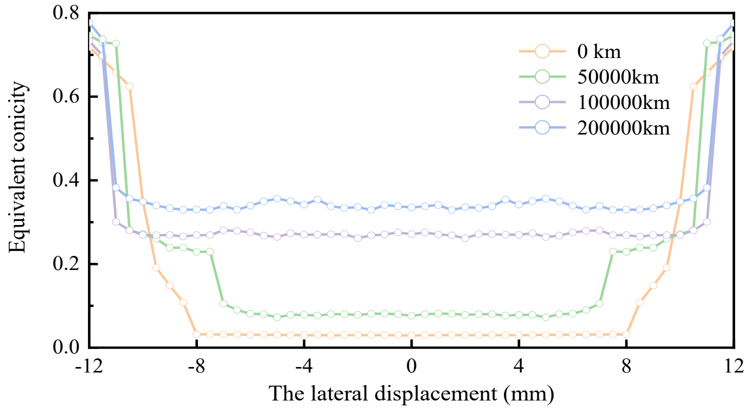

Fig. 5. Calculated equivalent conicity at different service mileages.

Utilizing the Curve Fitting Toolbox in MATLAB, a Gaussian fitting approach was implemented to derive nonlinear expressions for the equivalent conicity relative to wheelset lateral displacement across various service mileages.

Specifically, for the service mileage of 50,000 km, the equivalent conicity curve was fitted using a six-term Gaussian function. The resulting fitted representation is as follows:

$$\begin{aligned}\lambda(y) = {} & 1.247e^{-\left(\frac{y-11.53}{0.5677}\right)^2} + 0.007813e^{-\left(\frac{y+13.52}{0.03744}\right)^2} + 2.67e^{-\left(\frac{y+11.5}{0.3715}\right)^2} \\ & -0.2026e^{-\left(\frac{y+5.154}{4.405}\right)^2} + 0.3391e^{-\left(\frac{y+9.564}{10.3}\right)^2} + 0.2561e^{-\left(\frac{y-9.509}{2.857}\right)^2}\end{aligned} \tag{2}$$

The Sum of Squares due to Error (SSE) is 0.01645, and the coefficient of determination (R-square) is 0.9897.

The equivalent conicity curve for the service mileage of 100,000 km was fitted using a five-term Gaussian function. The resulting numerical representation is as follows:

$$\lambda(y) = 0.6132e^{-\left(\frac{y-11.77}{0.4409}\right)^2} + 0.6142e^{-\left(\frac{y+11.77}{0.4399}\right)^2} + 0.271e^{-\left(\frac{y+33.61}{2646}\right)^2} \tag{3}$$

The SSE is 0.000967, and the R-square is 0.9987.

The equivalent conicity curve for the service mileage of 200,000 km was fitted using a three-term Gaussian function. The resulting numerical representation is as follows:

$$\lambda(y) = 0.545e^{-\left(\frac{y+11.77}{0.4844}\right)^2} + 0.5451e^{-\left(\frac{y-11.77}{0.4839}\right)^2} + 0.34e^{-\left(\frac{y-34.93}{3417}\right)^2} \tag{4}$$

The SSE is 0.0033, and the R-square is 0.9948.

The fitting results demonstrate that the proposed equivalent conicity functions for each service mileage exhibit a high degree of consistency with the raw data. Evaluation metrics indicate superior model fidelity: the SSE remains below 0.02, while the R-square exceeds 0.98, both falling well within acceptable scientific tolerances. This effectively validates that the proposed model possesses excellent fitting performance and predictive accuracy across the entire spectrum of service mileages.

A two-degree-of-freedom wheelset system model comprising lateral and yaw motions is established as depicted in Fig. 6, assuming no constraints from the bogie frame. To capture the nonlinear contact mechanics, the model integrates an exponential approximation for the interface geometry and utilizes Kalker's linear theory for creep force estimation. The normal force's impact is quantified through gravitational restoring stiffness in both lateral and yaw directions. Applying Newton's second law, the nonlinear lateral stability of the wheelset is mathematically represented by a series of nonlinear ordinary differential equations. [12]:

$$\begin{cases} m\ddot{y} - \dfrac{2f_{22}}{v}\dot{y} + (K_{1y} + \dfrac{W\lambda(y)}{b})y - 2f_{22}\psi + F_t(y) = 0 \\ J\ddot{\psi} + \dfrac{2f_{11}b^2}{v}\dot{\psi} + \dfrac{2f_{11}b\lambda(y)}{r_0}y + (K_{1x}b_1^2 - Wb\lambda(y))\psi = 0 \end{cases} \tag{2-5}$$

where y is the lateral displacement, and ψ is the yaw angle. The physical meaning and numerical values of the other parameters are provided in Table 1.

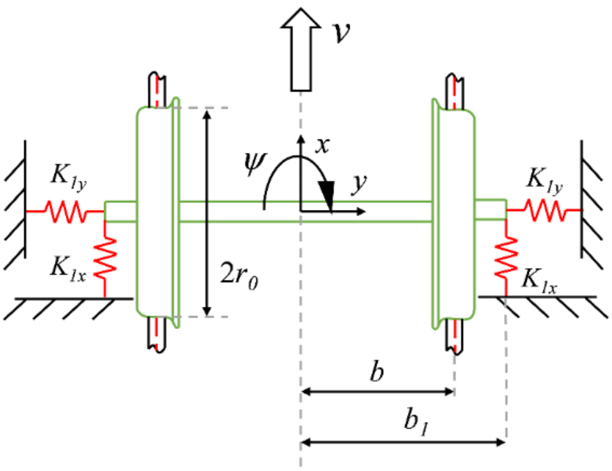

Fig. 6 Wheelset System Model

Tab.1 Wheelset Model Parameters

Parameter	Name	Value	Unit
m	Mass of the wheelset	1780	kg
J	Yaw moment of inertia of the wheelset	967	kg·m^2
r_0	Centered wheel rolling radius	0.43	m
b	Half of the lateral distance of the rolling circle	0.7465	m
b_1	Half of the swing arm	1.0	m
v	Train speed	/	m/s
K_{1x}	Primary lateral stiffness	2	MN/m
K_{1y}	Primary lateral stiffness	2	MN/m
f_{11}	Longitudinal creep coefficient	1.5	MN
f_{22}	Lateral creep coefficient	1.5	MN
W	Axle load	70	kN

3 Results

The velocity-related parameter is selected as the critical bifurcation parameter. Based on nonlinear dynamics theory, a Hopf bifurcation occurs when the Jacobian matrix of the system possesses a pair of purely imaginary eigenvalues at the equilibrium point, while all remaining eigenvalues have negative real parts. This bifurcation is categorized into supercritical or subcritical types, depending on the sign of the first Lyapunov coefficient. By perturbing the bifurcation parameter within the neighborhood of its critical value and examining the sign of the Lyapunov coefficient, one can determine the stability characteristics of the system's solutions and the laws governing the evolution of its topological structure [13]. The numerical computations in this study are primarily conducted using the MATCONT software package [14].

By incorporating the equivalent conicity data from various service mileages into the established single-wheelset model—which accounts for nonlinear equivalent conicity and flange forces—the Hopf limit cycles of the nonlinear wheelset system are obtained, as illustrated in Fig. 7. Correspondingly, the Hopf bifurcation speeds, nonlinear critical speeds, and first Lyapunov coefficients for the system across different mileages are summarized in Table 2. It is noted that when the initial LMA wheel profile is employed, the system exhibits relatively small equivalent conicity, leading to a higher hunting speed; therefore, its corresponding Hopf bifurcation diagram is not presented in this study.

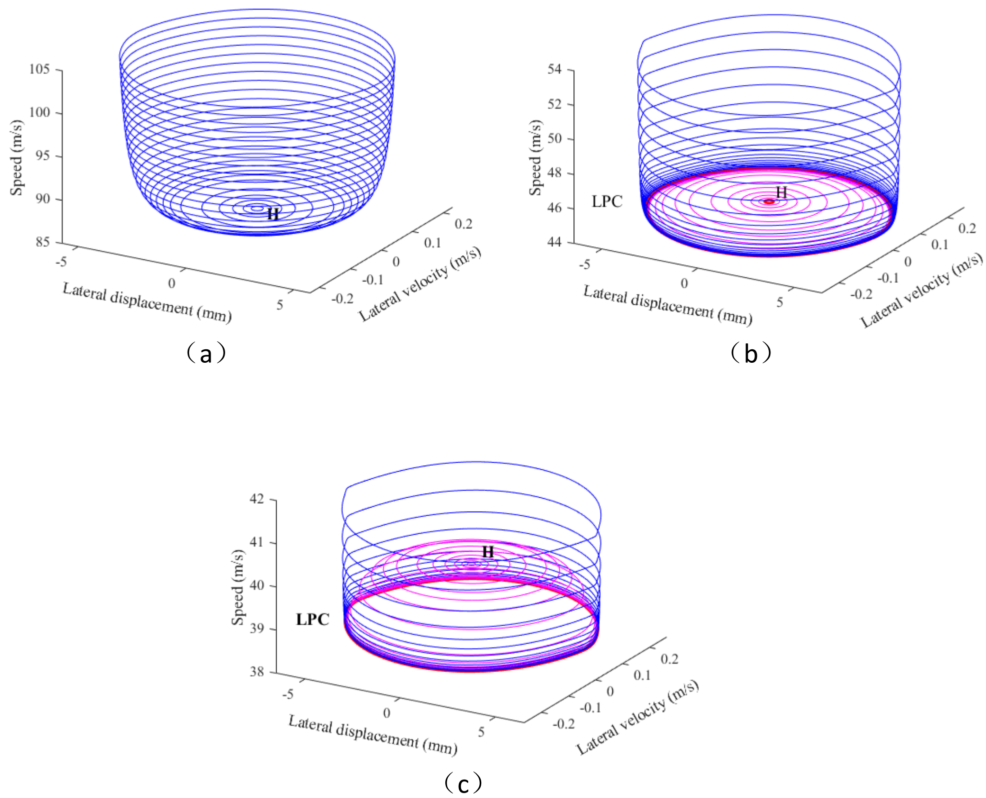

Fig. 7. Hopf bifurcation limit cycles of the wheelset system at characteristic sections: (a) 50,000 km; (b) 100,000 km; (c) 200,000 km.

Based on the bifurcation analysis results, the single-wheelset system exhibits a supercritical Hopf bifurcation at a service mileage of 50,000 km, whereas subcritical Hopf bifurcations occur at mileages of 100,000 km and 200,000 km. A comparative analysis of the Hopf bifurcations alongside the wheel-rail contact relationships reveals that for mileages of 0 km, 50,000 km, and 100,000 km, the contact points remain localized on the tip of the switch rail across various lateral displacements. At 50,000 km, the system's Hopf bifurcation speed is recorded at 86.92 m/s. As the mileage increases from 50,000 km to 100,000 km, the equivalent conicity of the wheel-rail system undergoes a substantial increment, causing the Hopf bifurcation speed of the nonlinear wheelset to drop by nearly half, reaching 45.37 m/s. As the service mileage further extends from 100,000 km to 200,000 km, the continued evolution of wheel wear causes the wheel-rail contact points to shift, distributing between the switch rail and the stock rail at different lateral displacements. During this stage, the increase in equivalent conicity is relatively minor; consequently, the Hopf bifurcation speed at 200,000 km decreases slightly further to 40.10 m/s.

Table 2. Hopf bifurcation analysis of the single-wheelset system at different service mileages.

Switch rail head width (km)	Hopf bifurcation speed V_H (m/s)	Nonlinear critical speed $V_{nonlinear}$ (m/s)	First Lyapunov coefficient
50,000	86.92	/	-1.75
100,000	45.37	44.75	0.52
200,000	40.10	38.70	0.70

It is noteworthy that at shorter service mileages such as 50,000 km, the Hopf bifurcation speed remains high due to the limited wheel wear. However, as wear accumulates, particularly when the mileage reaches 100,000 km or 200,000 km, the bifurcation speed exhibits a significant decline compared to the initial 50,000 km case. The evolution of the wheel profile with increasing operational mileage leads to substantial alterations in the wheel-rail contact relationship during the initial stage of wear spanning from 0 km to 100,000 km. In this period, the equivalent conicity of the system undergoes a pronounced variation, which in turn causes a sharp reduction in the bifurcation speed and adversely affects the lateral stability of the wheelset.

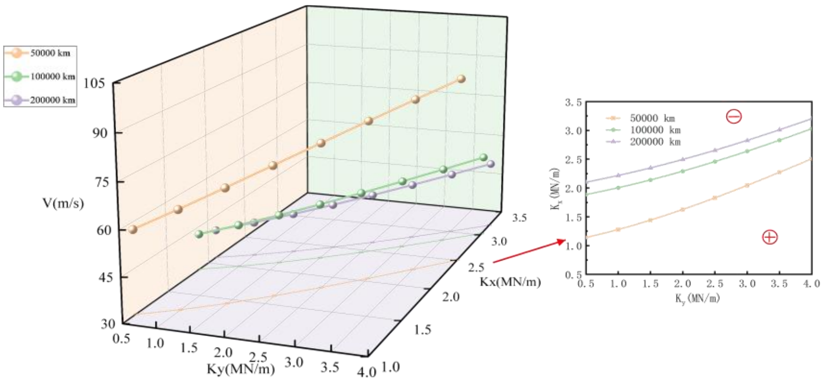

Fig. 8. Evolution of the bifurcation-type critical line in the k_x-k_y parameter space considering wheel profile evolution

In a two-parameter bifurcation space, the locus where the first Lyapunov coefficient vanishes is typically defined as the bifurcation-type critical line. This characteristic curve partitions the entire parameter domain into two distinct regions with differing dynamical properties, corresponding to supercritical and subcritical Hopf bifurcations, respectively. Notably, parameter combinations situated on this critical boundary lead to the occurrence of degenerate Hopf bifurcations in the single-wheelset system. Through numerical computations, this study identifies the distribution and evolution of Hopf bifurcation types within the dual-parameter space across various service mileages. Figures 8, 9, and 10 illustrate the evolution of these critical lines within the parameter spaces defined by primary longitudinal vs. lateral stiffness, primary longitudinal stiffness vs. longitudinal creep coefficient, and longitudinal vs. lateral creep coefficients, respectively. Within these parameter planes, the critical line divides the total space into two segments, denoted as Region ⊕ and Region ⊖. In Region ⊕, the first Lyapunov coefficient is positive, corresponding to the subcritical Hopf bifurcation domain, whereas in Region ⊖, the coefficient is negative, thereby representing the supercritical Hopf bifurcation domain.

As illustrated in Fig. 8, with the increase in wheel service mileage, both the primary longitudinal and lateral stiffness values corresponding to the bifurcation-type critical line exhibit an approximately linear growth relationship. The growth rates of these critical lines across different service mileages are remarkably consistent. Furthermore, by selecting points along the direction of increasing primary longitudinal stiffness on the critical line, it is observed that the critical speeds at which the degenerate Hopf bifurcation occurs in the single-wheelset system show a gradual upward trend for all considered mileages

During the optimization of suspension parameters, a combination of higher primary longitudinal stiffness and lower primary lateral stiffness should be prioritized. This configuration ensures that the system maintains supercritical Hopf bifurcation characteristics during hunting instability, effectively preventing abrupt transitions in the vehicle's dynamic state. Within the same parameter space, considering that the supercritical Hopf bifurcation domain undergoes a more significant contraction as wheel wear increases during the initial stages (up to 100,000 km), special attention must be paid to the distribution of the bifurcation-type critical line between 50,000 km and 100,000 km of service mileage. By appropriately designing the primary longitudinal and lateral stiffness, the wheelset can be maintained within the supercritical Hopf bifurcation domain even during early wear stages, thereby mitigating the risk of lateral instability and enhancing overall operational safety.

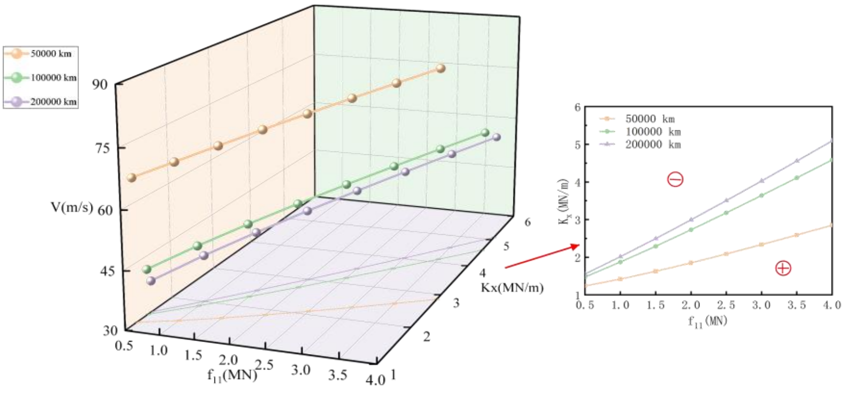

Fig. 9. Evolution of the bifurcation-type critical line in the k_x-f_{11} parameter space considering wheel profile evolution.

Based on the evolution of the bifurcation-type critical line within the parametric space of primary longitudinal stiffness and longitudinal creep coefficient shown in Fig. 9, it can be observed that both k_x and f_{11} corresponding to the critical line exhibit an approximately linear growth relationship across different service mileages. By selecting points along the direction of increasing longitudinal creep coefficient on the critical line, the critical speeds at which the single-wheelset system undergoes degenerate Hopf bifurcation also show an approximately linear upward trend, with consistent rates of change observed for all mileages. Regardless of the service mileage, a higher primary longitudinal stiffness combined with a lower longitudinal creep coefficient is more conducive to maintaining the system within the supercritical Hopf bifurcation domain. Therefore, during system parameter design, emphasis should be placed on the distribution of the critical line during the initial wear stages (50,000 km to 100,000 km). By reasonably selecting values for k_x and f_{11}, the system should be optimized to remain within the supercritical Hopf bifurcation domain across the entire service life.

According to the evolution of the bifurcation-type critical line in the f11-f22 parameter space shown in Fig. 10, the longitudinal and lateral creep coefficients corresponding to the critical line exhibit an approximately linear decrease across different service mileages. Furthermore, by selecting points along the direction of increasing lateral creep coefficient on the critical line, the critical speeds for the occurrence of degenerate Hopf bifurcation show an approximately linear growth trend, with the rate of change remaining identical across all mileages. Regardless of the service mileage, lower longitudinal and lateral creep coefficients are more conducive to maintaining the system within the supercritical Hopf bifurcation domain. Consequently, during system parameter design, emphasis should be placed on the distribution of the critical line during the initial wear stages (50,000 km to 100,000 km). Rational selection of creep coefficients is essential to ensure that the system remains within the supercritical Hopf bifurcation domain throughout various operational stages.

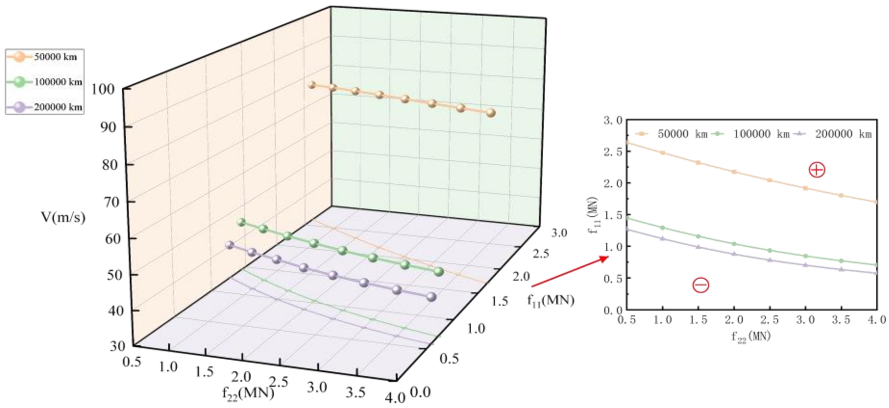

Fig. 10. Evolution of the bifurcation-type critical line in the f_{11}-f_{22} parameter space considering wheel profile evolution.

4 Conclusions and Contributions

To elucidate the hunting motion and bifurcation characteristics of wheelsets under characteristic switch rail profiles across varying service mileages, this study utilizes an equivalent conicity calculation method derived from the wheelset hunting wavelength formula. This approach provides a robust theoretical framework for enhancing turnout speeds, optimizing rail profiles, and refining vehicle system parameters. Within the context of nonlinear dynamics, a nonlinear single-wheelset model for the switch zone is formulated, integrating nonlinear wheel-rail contact geometry and flange forces. Taking the 35 mm head-width profile as a representative case, the study quantifies the impact of wheel profile evolution on the system's bifurcation behavior.

Equivalent-conicity analysis reveals a significant mileage-driven augmentation within the relevant lateral displacement range, with more pronounced increments observed beyond 100,000 km. Correspondingly, bifurcation results manifest a substantial attenuation of the hunting onset speed as mileage accumulates, dropping from 86.92 m/s at 50,000 km to 40.10 m/s at 200,000 km. Crucially, a qualitative transition in the Hopf bifurcation type is identified: early-mileage profiles (up to 50,000 km) exhibit a supercritical onset characterized by continuous amplitude growth , whereas late-mileage profiles (from 100,000 km to 200,000 km) transition to a subcritical onset. The latter is marked by jump-type emergence and hysteresis, underscoring a heightened sensitivity to disturbances near the stability threshold. Two-parameter bifurcation maps further show that the boundary separating supercritical and subcritical regimes shifts with mileage, indicating that the interaction between suspension stiffness and creep effects governs both the stability margin and the instability mode. This coupled mechanism evolves systematically with wear accumulation.

Acknowledgements

The authors acknowledge the financial support provided by the National Natural Science Foundation of China (U2568212, 52388102, 52478474, 52472458).

References

[1] Wang P, Xu J, Wang S, et al. A review of research on design theory and engineering practice of high-speed railway turnout[J]. Intelligent Transportation Infrastructure, 2022, 1.

[2] Li T, Xiang K, Yan Z, et al. Effect of operating conditions on the time-frequency characteristic of high-speed vehicle-turnout dynamic interaction using synchrosqueezed wavelet transform[J]. Vehicle System Dynamics, 2024: 1-23.

[3] Wang C, Dai H, Wang J, et al. Experimental and simulation study on the effect of different wheel profiles on the dynamics and wheel wear of high-speed trains[J]. Proceedings of the Institution of Mechanical Engineers, Part F: Journal of Rail and Rapid Transit, 2023, 237(8): 1025-1036.

[4] Hou M, Chen B, Cheng D. Study on the evolution of wheel wear and its impact on vehicle dynamics of high-speed trains[J]. Coatings, 2022, 12(9): 1333.

[5] Chen R, Chen J, Wang P, et al. Impact of wheel profile evolution on wheel-rail dynamic interaction and surface initiated rolling contact fatigue in turnouts[J]. Wear, 2019, 438: 203109.

[6] Hao C, Chen J, Sun X, et al. Effects of flange wear on dynamic vehicle-turnout interaction[J]. Proceedings of the Institution of Mechanical Engineers, Part F: Journal of Rail Rapid Transit, 2023, 237(5): 642-654.

[7] Shi H, Wang J, Wu P, et al. Field measurements of the evolution of wheel wear and vehicle dynamics for high-speed trains[J]. Vehicle System Dynamics, 2018, 56(8): 1187-1206.

[8] Wang J, Ling L, Wang K, et al. Nonlinear stability evolution of railway wagon system due to wheel profile wear[J]. Nonlinear Dynamics, 2024, 112(14): 11971-11991.
[9] Liu B, Bruni S. Influence of individual wheel profiles on the assessment of running dynamics of a rail vehicle by numerical simulation: a case study[J]. Vehicle System Dynamics, 2021, 60(7): 2393-2412.
[10] Guo J, Shi H, Luo R, et al. Bifurcation analysis of a railway wheelset with nonlinear wheel–rail contact[J]. Nonlinear Dynamics, 2021, 104(2): 989-1005.
[11] Qian Y, Wang P, Xie K, et al. Development and application of a calculation method for the equivalent conicity in high-speed turnout Zones[J]. Vehicle system dynamics, 2022, 60(1): 96-113.
[12] Ge P, Wei X, Liu J, et al. Bifurcation of a modified railway wheelset model with nonlinear equivalent conicity and wheel–rail force[J]. Nonlinear Dynamics, 2020, 102(1): 79-100.
[13] Zhang T, Dai H. On the nonlinear dynamics of a high-speed railway vehicle with nonsmooth elements[J]. Applied Mathematical Modelling, 2019, 76: 526-544.
[14] Dhooge A, Govaerts W, Kuznetsov Y A. MATCONT: a MATLAB package for numerical bifurcation analysis of ODEs[J]. ACM Transactions on Mathematical Software, 2003, 29(2): 141-164.